Diffusion of Water in Cat Ventricular Myocardium

ROBERT E. SAFFORD, E. ANNE BASSINGTHWAIGHTE, and JAMES B. BASSINGTHWAIGHTE

From the Department of Physiology and Biophysics, Mayo Graduate School of Medicine and Mayo Medical School, Rochester, Minnesota 55901. Dr. Safford's present address is Department of Internal Medicine, Massachusetts General Hospital, Boston, Massachusetts 02114; Dr. James B. Bassingthwaighte's present address is Center for Bioengineering, University of Washington, Seattle, Washington 98195.

ABSTRACT The rates of diffusion of tritiated water (THO) and [^{14}C]sucrose across cat right ventricular myocardium were studied at 23°C in an Ussing-type diffusion cell, recording the time-course of increase in concentration of tracer in one chamber over 4–6 h after adding tracers to the other. Sucrose data were fitted with a model for a homogeneous sheet of uneven thickness in which the tissue is considered to be an array of parallel independent pathways (parallel pathway model) of varying length. The volume of the sucrose diffusion space, presumably a wholly extracellular pathway, was 23% of the tissue or 27.4 ± 1.7% (mean ± SEM; n = 11) of the tissue water. The effective intramyocardial sucrose diffusion coefficient, D_s, was 1.51 ± 0.19 × 10^{-6}cm^2·s^{-1} (n = 11). Combining these data with earlier data, D_s was 22.6 ± 1.1% (n = 95) of the free diffusion coefficient in aqueous solution D_s^c. The parallel pathway model and a dead-end pore model, which might have accounted for intracellular sequestration of water, gave estimates of D_w/D_w^c (observed/free) of 15%. Because hindrance to water diffusion must be less than for sucrose (where D_s/D_s^c = 22.6%), this showed the inadequacy of these models to account simultaneously for the diffusional resistance and the tissue water content. The third or cell-matrix model, a heterogeneous system of permeable cells arrayed in the extracellular matrix, allowed logical and geometrically reasonable interpretations of the steady-state data and implied estimates of D_w in the cellular and extracellular fluid of ~ 25% of the aqueous diffusion coefficient.

INTRODUCTION

Water fluxes in organs are governed by hydrodynamic and osmotic forces. The interpretation of tracer and bulk water movements is becoming more complex as our understanding improves, and requires increasingly detailed knowledge of tissue geometry and of the conductances of the different tissue components. These conductances include intracellular and extracellular diffusion, permeation of membranes, and flow in the vascular system, and perhaps, in the extravascular region. There is a possibility that some tissue water is partially immobilized or otherwise inhibited from exchanging rapidly and that the driving forces for water fluxes are influenced by such sequestration.

Intratissue diffusion of water in muscle has been assumed to be so rapid that

it can be used as an indicator for the intratissue distribution of blood flow (Thompson et al., 1959; Paradise et al., 1971). Yipintsoi and Bassingthwaighte (1970) showed that water and iodoantipyrine dilution curves obtained simultaneously from dog hearts differed slightly, and interpreted this to suggest that water diffused more rapidly than iodoantipyrine and partook in some arteriovenous diffusional shunting. Rose et al. (1977) conducted refined experiments using the multiple indicator dilution technique, also in dog hearts, and observed changes in the shape of the tritiated water curves between vasoconstricted and vasodilated states. They attribute the differences to a limitation in the conductance in the extravascular region, specifically to barrier limitations at both the capillary and sarcolemmal membranes. Their analyses are based on assumptions that diffusion in interstitial fluid and inside cells is rapid and that diffusion distances are short.

Preliminary studies of the diffusion of water in the myocardium have suggested that the overall effective diffusion coefficient is about one-quarter (Suenson et al., 1974; Safford and Bassingthwaighte, 1977) to one-half (Page and Bernstein, 1964) of the free diffusion coefficient in water. Page and Bernstein argued that tracer water took primarily an extracellular path and leaked into cells so slowly that cytoplasmic water acted as a dead-end pore volume; this interpretation is not compatible with the more recently obtained indicator dilution data of Yipintsoi and Bassingthwaighte (1970) and Rose et al. (1977). Suenson et al. (1974) could not fit the data with a dead-end pore model (adapted from Goodknight and Fatt, 1961) and reasoned that the sarcolemmal water permeability was therefore quite large and that the water flux in cardiac muscle passes through both the extracellular space and across myocardial sarcolemma, diffusing through the cells.

In this study, with much more extensive data than previously available, the analysis showed that neither the homogeneous sheet model nor the dead-end pore model, both adapted for a sheet of uneven thickness, could provide reasonable estimates of the intramyocardial diffusion coefficient or diffusion space for water. The key to this conclusion was using an intimately related reference tracer, sucrose, as an inbuilt control for the water study.

This failure of the previous models for extracellular diffusion to apply to data for water, which permeates cells and diffuses through them, forced the develoment of a heterogeneous cell-matrix model. We used the same basic concepts as Redwood et al. (1974) and Stroeve et al. (1976) in considering tracer diffusion across a planar slab of tissue considered macroscopically homogeneous but microscopically heterogeneous. The model accounts for diffusion intra- and extracellularly and for finite sarcolemmal permeability on all surfaces of the cells. The equations are new inasmuch as the model of Redwood et al. did not account for finite intercellular distances along the diffusion gradient, and that of Stroeve et al. was for isolated suspended spheres, and would need to be extended to cylinders or parallelopipeds.

MATERIALS AND METHODS

In 19 experiments we have excised the upper anterior wall of the right ventricle of small cats and kittens (0.6–1.5 kg) anesthetized with sodium thiamylate and clamped the muscle

sheet between the chambers of an Ussing-type diffusion cell so that a relatively smooth circular sheet of muscle 0.6 cm in diameter (total area [A_T] = 0.283 cm^2) is exposed to Krebs-Ringer solution on both surfaces, as described in more detail by Suenson et al. (1974). The Krebs-Ringer solution contained (in millimolar): Na 147, K 5.4, Ca 1.8, Mg 0.5, Cl 133, HCO_3 24, H_2PO_4 0.4, glucose 2.2, at pH 7.4. To minimize the unstirred layer

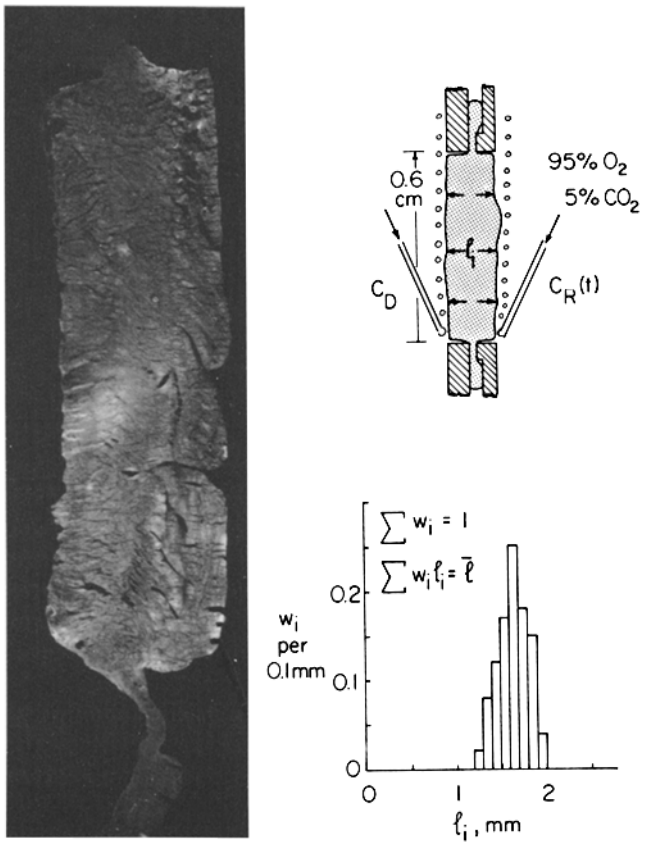

FIGURE 1. Left panel: photograph of frozen section of muscle sheet cut perpendicular to its plane. Right upper panel: diagram of muscle sheet in chamber. The Lucite compression ring holding the perimeter of the muscle sheet is cross-hatched. Petroleum jelly coats the surface of the lucite clamping the tissue. The diameter of the disk of muscle is 0.6. The l_i are the thicknesses of the sheet. Right lower panel: frequency distribution (w_i) of measurements of tissue thickness (l_i) taken 200 μm apart along the full widths of six sections, a total of 180 measurements. The distribution of l_i's for the sheet shown in the left panel was narrower than this.

at the solution-tissue interface, the solution in each chamber (14.5 cm^3 in volume) was agitated by a magnetic stirring bar, and the tissue was oxygenated on both surfaces by streams of bubbles (95% O_2, 5% CO_2) sweeping upwards. (See Fig.1, right upper panel.) All of the experiments were performed at room temperature 21–23°C. The electrical resistance of the muscle sheet, shown to be an index of tissue viability by Suenson et al.

(1974), was measured once each hour using a voltage clamp circuit similar to that described by LaForce (1967). The fractional water content, f, (gram of H_2O/gram of wet muscle) of a piece of right ventricular free wall adjacent to the tissue used in the diffusion cell was determined from the weight loss of the tissue in an oven at 100°C after 48 h as described by Yipintsoi et al. (1972).

After allowing 1 1/2–2 h for equilibration of the tissue with the bathing media, tritiated water (50 μCi), $^{45}CaCl_2$ (300 μCi) and in 11 of 19 experiments [^{14}C]sucrose (200 μCi) (all purchased from New England Nuclear, Boston, Mass.) were added at high specific activity to the chamber facing the epicardial surface of the muscle sheet ("donor" chamber). Samples (200 μl) were taken at regular intervals of time t (2–15 min) after addition of tracers from the chamber facing the endocardial surface of the tissue ("recipient" chamber) using an adjustable pipette with disposable polyethylene tips for at least the next 6 h in most experiments and were replaced with an equal volume of unlabeled solution to maintain equality of hydrostatic pressures across the muscle sheet. Duplicate samples were taken from the donor chamber at the start and end of the experiment.

The samples were counted in a Nuclear-Chicago Mark II 3-channel liquid scintillation counter (Nuclear-Chicago Corp., Des Plaines, Ill.) with windows set to discriminate between ^{3}H, ^{14}C, and ^{45}Ca. (The ^{45}Ca curves were part of a large study previously reported by Safford and Bassingthwaighte [1977] and will not be mentioned further.) For all but the first few samples of an experiment the samples were counted for long enough to accumulate at least 10,000 counts per sample in each channel giving <1% counting error. The activity of each tracer in each sample was obtained, as described in detail by King and Bassingthwaighte (1978), using an automatic external standard method for ascertaining the effects of quenching on background count rates, on efficiencies, and on spillover rates, and allowing the application of a matrix inversion approach to solving the three equations for the three unknowns. The counts were corrected for the tracer removed with each 200-μl sample, giving us as a final result the concentration of each of the three tracers in the recipient chamber as a function of time; curves for sucrose and water are illustrated in Fig. 2. The abscissal intercepts are the time lags, T.

At the end of an experiment the muscle sheet was removed from the diffusion cell, carefully but rapidly frozen on a block of dry ice to preserve its dimensions, and sliced perpendicular to the plane of the sheet on a refrigerated microtome. Five to six slices of the general form shown in Fig. 1, left panel, taken ~ 0.5 mm apart near the center of the circular disk of muscle, were stained with a 0.1% solution of Toluidine Blue and examined using the × 3.5 objective of a light microscope with a micrometer eyepiece. The thickness from epicardium to endocardium was measured at 200-μm intervals across the full width of each section, providing 150–180 estimates of thickness and enabling a histogram of the tissue thickness distribution to be constructed for each sheet, as illustrated in Fig. 1, right lower panel. Inasmuch as these slices did not cover the entire sheet, it was assumed that the thicknesses were representative of the remaining one-third to one-half of the tissue. The average thickness is $\bar{l}$.

ANALYTICAL METHODS

A glossary of terms is provided in Appendix I. The equations for diffusion across a sheet of uneven thickness are in Appendix II. Eq. II.4 of Appendix II gives the modification of the Goodknight and Fatt (1961) dead-end pore equation to the nonuniform sheet. This modification was used by Safford and Bassingthwaighte (1977) to estimate the diffusion coefficient for Ca^{++} in the presence of myocardial ionic binding sites, where the number of Ca^{++} binding sites (dead-end pore volume) depended upon the ionic

milieu. From the steady-state data (linear portion of the curve, Fig. 1) the observed diffusion coefficient, D, and the area of the diffusion pathway, A_d, were calculated as follows:

$$D = \frac{V_d(1 + V_{dep}/V_d)}{6TA_d \sum_{i=1}^{N} \frac{w_i}{l_i}} \tag{1}$$

$$A_d = \frac{\frac{dC_R'}{dt} V}{D \sum_{i=1}^{N} \frac{w_i}{l_i}}, \tag{2}$$

where $V_d = \dot{l}A_d$. A third equation develops from requiring that the sum of V_d and V_{dep} equal the total tissue water, V_w:

$$V_w = A_T \dot{l} \rho f = V_d + V_{dep} \tag{3}$$

or

$$V_{dep} = \dot{l}(A_T \rho f - A_d). \tag{4}$$

D, A_d and V_{dep}, the three parameters present in a steady-state solution, are determined by solving Eqs. 1, 2, and 4 simultaneously. The density of water at 25°C has been taken to

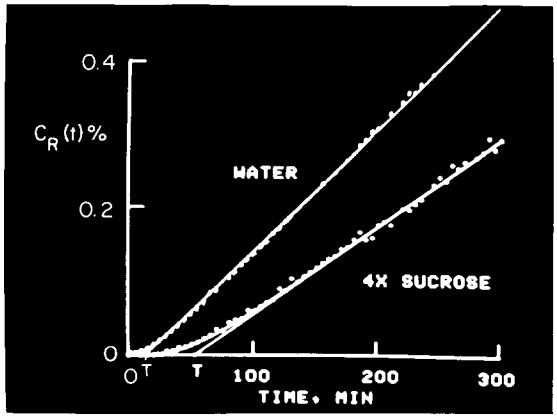

FIGURE 2. Diffusion curves $[C_R(t)]$ for tritiated water and for [^{14}C]sucrose (scaled to four times actual values). Straight lines have been fitted to the steady-state (linear) regions of the curves and extrapolated to define the time lags T. (13 min for THO and 56 min for [^{14}C]sucrose). The homogeneous sheet model (Eq. II.1 of Appendix II) has been fitted to the curves using, for THO, $D_w = 5.5 \times 10^{-6}$cm^2·s^{-1} and $A_{dw}/A_T = 0.58$ and, for [^{14}C]sucrose, $D_s = 2.35 \times 10^{-6}$cm^2·s^{-1} and $A_{ds}/A_T = 0.25$.

be 1 g/ml; f is the fractional water content in gram/gram wet tissue and was measured in each experiment; ρ, the density of the wet tissue, has been taken to be 1.053 g/ml (Suenson et al., 1974).

The shapes of the transient portions of the water curves provide estimates of a rate constant, k_e, for exchange between V_d and V_{dep}. the values of D, A_d, and V_{dep} computed from the steady-state were substituted into Eq. II.4 of Appendix II, and the value of k_e

was adjusted until the curvature of the computed $C'_R(t)$ matched that of the data as shown in Fig. 3. From k_e, the sarcolemmal water permeability P_w may be estimated by assuming V_{dep} to be the sarcoplasmic water space.

CELL PERMEATION MODEL

We have developed a model in the style of Redwood et al. (1974) leading to a set of new equations that can be applied to intramyocardial diffusion. To do so we have idealized the description of myocardial histology provided by Streeter et al. (1969) as shown in Fig. 4. We imagine myocardial cells to be long square-ended parallelepiped of width $L \times L$ separated by extracellular space of thickness L_o such that they form a cubic lattice. The long axes of the cells are perpendicular to the direction of diffusion (z coordinate), and the ends are assumed to be apposed to the ends of adjacent cells, as by intercalated disks, so

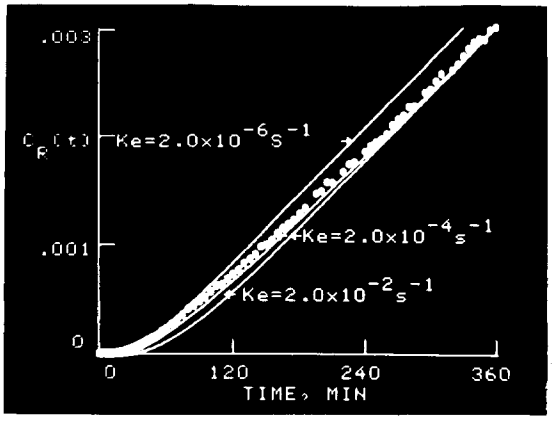

FIGURE 3. Dead-end pore model for water diffusion. Illustration of effect of k_e, the rate constant for exchange between diffusion channel and dead-end pore volume, on curvature of transient for dead-end pore model. At high k_e, equilibration is rapid and the transient short (~ 150 min); at intermediate k_e, the transient extends for ~ 5 h. At low k_e, $2 \times 10^{-6} s^{-1}$ the transient is far from complete at 6 h, although the curve from 3 to 6 h appears deceptively straight. The final steady-state slope and intercept are the same in all cases.

that axial diffusion is zero. The surface-to-volume ratio of the cells is $4/L$; this ratio is felt appropriate for any long cells of regular shape and is the same for hexagons, octagons, and circles when L is defined as the distance between diametrically opposed sides. The volume of each element per unit length of the matrix, dashed square in Fig. 4, is $(L + L_o)^2$, so that the ratio of cell surface to elemental volume is $4L/(L + L_o)^2$.

The fraction, V_e, of tissue that is occupied by extracellular fluid is

$$V_e = 1 - L^2/(L + L_o)^2. \tag{5}$$

Diffusional flux in the z direction occurs via two pathways in parallel: through the extracellular fluid (ECF) pathway (A in Fig. 4), and through the cells and ECF in series (pathway B in Fig. 4); exchange between these pathways occurs at

all points. Lateral equilibration is assumed to be instantaneous within each region, but not across the membranes. Permeation occurs through the cell sides as well as through the top and bottom. [The model of Redwood et al. (1974) assumed the extracellular path length L_o in pathway B to be zero.] D_e and D_i are the extracellular and intracellular tracer diffusion coefficients for water, respectively; P is the permeability of the sarcolemma to tritiated water, and is assumed to be the same on all sides. The equations developed in Appendix III provide the overall bulk diffusion coefficient D_b:

$$D_b = D_e\left\{\left(\frac{L_o}{L + L_o}\right) + \left[L\left(\frac{D_i}{D_e}\right)(W\alpha K - Q) - L_o(\alpha K + Q)\right]^{-1}\right\}^{-1}, \tag{6}$$

where the permeability P is contained in the constants α, K, and Q, given in Appendix III. In the limits this expression is simpler. The lower limit obtained when $P = 0$ or $D_i = 0$ is

$$D_b(P = 0) = D_e \cdot \frac{L_o(L + L_o)}{L(L + L_o) + L_o^2}. \tag{7}$$

The upper limit occurs when there is no barrier to permeation:

$$\begin{aligned} D_b(P = \infty) &= \frac{1}{\dfrac{L}{LD_i + L_oD_e} + \dfrac{L_o}{(L + L_o)D_e}} \\ &= \frac{D_e(L + L_o)(D_i + L_oD_e/L)}{D_e(L + L_o) + L_o(D_i + L_oD_e/L)}, \end{aligned} \tag{8}$$

and when $D_e = D_i$ and $P = \infty$, then $D_b = D_e$.

Eq. 6 was used to generate a series of plots of D_b vs. P such as Fig. 5 for various values of D_e, D_i, L, and L_o. As excepted when P is very small, D_b does not depend on D_i, the intracellular diffusion coefficient, and when P is large, D_b is a function of both D_e and D_i, inasmuch as both intracellular and extracellular fluxes are important.

From the steady-state slope of the experimental diffusion curve, (dC'_R/dt) for each experiment, we calculated D'_b from a first order Fick expression for the flux:

$$J_w = V(dC'_R/dt)_\infty = D'_bA_T(1 - C'_R)/\bar{l}, \tag{9}$$

or for the sheet of uneven thickness,

$$D'_b = \frac{V(dC'_R/dt)_\infty}{A_T(1 - C'_R)\sum_{i=1}^{i=N}(w_i/l_i)}. \tag{10}$$

Estimates of P could then be read from the plots of D_b vs. P, given specific assumptions concerning the geometries and the D's.

The models were fitted to the data under the control of SIMCON (Knopp et al., 1970), a simulation control system allowing us to display model solutions

superimposed on experimental data and to change model parameters between or during solutions.

RESULTS

The profile of a typical muscle sheet and the histogram of tissue thickness measurements corresponding to it are shown in Fig. 1. The weighting function, w_i, is the fraction of the total number of tissue thickness measurements for an experiment that is of magnitude l_i, and therefore, $\bar{l}$ is defined as

$$\bar{l} - \sum_{i=1}^{N} w_i l_i.$$

For solving the equations, an N of 5–10 classes of l_i sufficed for summarizing the 150–180 measurements, because further refinement of class sizes did not change

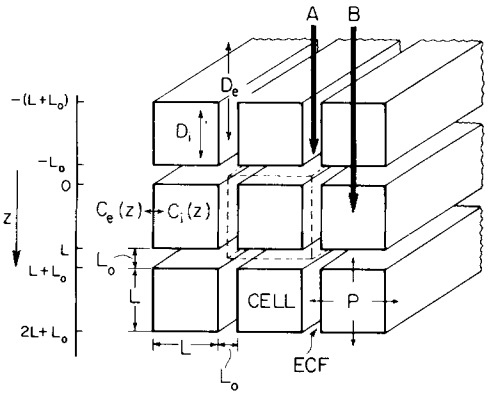

FIGURE 4. Geometric configuration of model for diffusion in the z direction. Cells are long square bars of cross-section L × L separated by an extracellular space of thickness L_o laterally and transversely. Extracellular and intracellular concentration profiles are $C_i(z)$ and $C_e(z)$. All four sides of the cells have equal permeability P. Diffusion is considered to be along two one-dimesional pathways in parallel and with exchange between them: instantaneous lateral equilibration is assumed in ECF and in cells; in addition, there is lateral exchange across the cell membrane from z = 0 to z = L as well as permeation at the upper and lower cell borders. D_e and D_i are extracellular and intracellular diffusion coefficients.

the shapes of the computed curves. Values of $\bar{l}$ ranged from 0.098 to 0.224 cm with an average of 0.159 cm. The relative dispersion of the tissue thickness measurements, defined as the standard deviation of $l_i/\bar{l}$, was computed for each experiment and ranged from 7.6 to 28.0%.

Table I summarizes the results of 19 experiments for which the homogeneous sheet and dead-end pore models were fitted to diffusion curves, $C_R'(t)$, for tritiated water. In 11 experiments the diffusion curve for a reference tracer, [^{14}C]sucrose, which does not penetrate the cells, was obtained simultaneously with the water curve in the same preparation; examples of the data are shown in

Fig. 2. The fractional water contents f average 0.85 ml/ml tissue or 0.81 g H_2O per gram tissue.

Sucrose

In order to provide estimates of extracellular diffusion coefficients and the volume of the diffusion channel uncompromised by permeation into cells, parameter values for sucrose curves were obtained from the parallel pathway homogeneous sheet model, and reported in Table I. From A_{ds}/A_T (by Eq. II.3), the measured $\bar{l}$'s and the measured fractional water contents, we estimate that

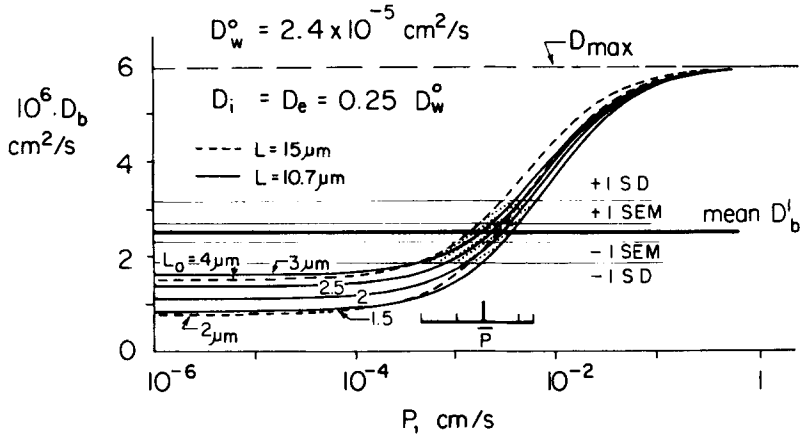

FIGURE 5. Solutions of the cell-matrix model for the interpretation of the observed bulk diffusion coefficient D'_b. Values of D'_b from Eq. 10 are demarcated by the horizontal lines giving the mean, ± 1 SEM and ± SD (n = 19). The curves are the theoretical D_b by Eq. 6. Two cell sizes were considered, diameters of 12 μm (L = 10.7 μm, continuous curves) and 17 μm (L = 15 μm, dashed curves). The extracellular space, V_e, was explored over a range of 0.2–0.4, defining L_o's from 2 to 4 μm for the 17-μm diameter cells and 1.5–3μm for the 12-μm diameter cells. The shaded area is the region of overlap of model and data. The possible range of P is given by the thick bar, with a mean estimate of ~ 2 × 10^{-3} cm/s based on a smooth cell surface or ~ 1.2 × 10^{-3} cm/s if cell surface irregularity and T tubular surface area are accounted for.

the sucrose diffusion channel occupies 27.4 ± 1.7% (mean ± SEM, n = 11) of the total tissue water volume.

The tracer diffusion coefficient of sucrose through the space calculated by Eq. II.2 was 29.6 ± 3.7% of that in water, and the tortuosities, λ_s, defined in Table I, averaged 1.96 ± 0.13. Suenson et al. (1974) found λ_s to be 2.11 ± 0.11 (mean ± SEM, n = 10) at 37°C, and Safford and Bassingthwaighte (1977) found it to be 2.34 ± 0.06 (n = 74) at 23°C. Summarizing all of our experience with sucrose diffusion, the mean ratio of observed to free diffusion coefficient, D_s/D°_s, from our three sets of data on cat right ventricular (RV) myocardium, was 22.6 ± 1.1% (SEM, n = 95).

Failure of the Homogeneous Sheet and Dead-End Pore Models of Water Diffusion

Parameter estimates were first obtained from the parallel pathway homogeneous sheet model. A_d/A_T for tritiated water, by Eq. II.3, was 57.5 ± 2.9% (mean ± SEM, n = 19), giving an apparent volume of the water diffusion channel, V_{dw}, equal to 67.4 ± 3.2% of the total tissue water, and over twice as large as V_{ds} for sucrose. D_w was estimated to be 3.59 ± 0.29 × 10^{-6}cm^2·s^{-1} (n = 19), which is 15.1% of the free tracer diffusion coefficient of water in a 150 mM NaCl solution (D_w°) at 25°C (McCall and Douglass, 1965).

Because the extracellular diffusion of water should not be more impeded than that for sucrose, the value of 15.1% and the V_{dw} larger than V_{ds} indicates water penetration through the cells with diffusion being impeded during transcellular passage. The parallel pathway dead-end pore model, fitted to data by using Eqs. II.4, 1, 2, and 4, provided the parameter estimates given in Table I. Using the same value of 0.575 for A_d/A_T as was obtained from the homogeneous sheet model gave estimates of the dead-end pore volume averaging 32.8 ± 3.2% of tissue water, thus accounting for 100% of the tissue water, as required

TABLE I

RESULTS OF FITTING MODELS TO WATER AND SUCROSE CURVES

Quantity	Homogeneous sheet model		Dead-end pore model for water	
	Sucrose	Water	V_{dw} variable	$V_{dw} = V_{ds}$
Tracer diffusion coefficient, $D \cdot 10^6$, $cm^2 \cdot s^{-1}$	1.51 ± 0.19	3.59 ± 0.29	3.79 ± 0.29	9.51 ± 0.73
D/D°, %	29.6 ± 3.7	15.1 ± 1.2	15.9 ± 1.2	40 ± 2.9
*Tortuosity, $\lambda = (D^\circ/D)^{1/2}$	1.96 ± 0.13	2.57 ± 0.11	2.51 ± 0.10	1.58 ± 0.12
Fraction of membrane area available for diffusion, A_d/A_T	0.233 ± 0.014	0.575 ± 0.029	0.575 ± 0.029	0.233 ± 0.014
Ratio of diffusion channel volume to total tissue water volume, V_d/V_w	0.274 ± 0.017	0.674 ± 0.032	0.674 ± 0.032	0.274 ± 0.017
Ratio of dead-end pore volume to total tissue water volume, V_{dep}/V_w	–	–	0.328 ± 0.032	0.726 ± 0.017
Rate constant for exchange between diffusion channel and dead-end pore, k_e, $s^{-1} \times 10^4$	–	–	4.3 ± 1.2	2.0 ± 0.6
Number of experiments	11	19	19	11

Mean ± SEM.

* D°_s = 5.10 × 10^{-6} cm^2·s^{-1} at 25°C (Irani and Adamson, 1958). D°_w = 2.38 × 10^{-5} cm^2·s^{-1} at 25°C (McCall and Douglass, 1965). f = 0.85g H_2O per gram tissue.

by Eq. 3. This model gave estimates of D_w/D_w° of 15.9 ± 1.2% (mean ± SEM, n = 19), and of the rate constant, k_e, for exchange between the diffusion channel and dead-end pore volume of 4.3 ± 1.2 × 10^{-4} s^{-1}. The standard error of the mean (as a fraction of the mean) of the estimates of k_e is much larger than those for the estimates of D_w, λ_w, and A_{dw}, because the curvature of the transient in Eq. II.4 is not a very strong function of k_e.

In the homogeneous sheet model the diffusion is assumed to occur everywhere in the sheet; in the dead-end pore model diffusion is only through the "diffusion channel", which is presumably extracellular. Inasmuch as both models gave D_w/D_w°'s of about 15%, which is low compared to the same ratio for sucrose, and inasmuch as A_d/A_T is larger than the extracellular space, which is close to or identical to V_{ds}, it appears that neither of these models is wholly appropriate for describing the diffusion of water in the myocardium. This

comment is a critical one because if sarcolemmal permeability were very low, the dead-end pore model would be adequate.

Application of the Heterogeneous Cell-Matrix Model

The "bulk" diffusion coefficient, D_b', from Eq. 10 is a direct interpretation of the steady-state slope $(dC_R'/dt)_\infty$ using the measured slab thicknesses, the chamber volume V of 14.5 ml, the total sheet area A_T of 0.283 cm^2, and the value of $C_R'(t)$ measured at the midpoint of the period over which the slope was measured. $C_R'(t)$ did not exceed 4% by the end of the experiments, so $1 - C_R'(t)$ was between 0.97 and 0.99. D_b' averaged $2.5 \pm 0.2 \times 10^{-6}$ cm^2/s. ($\pm$ SEM, n = 19), and 1 SD = 0.7×10^{-6} for the 19 experiments.

Use of the heterogeneous cell-matrix model required estimation of two geometric factors, L and L_o, two diffusivities, D_i and D_e, and the permeability P. The geometric factors are governed by the fractional volume of the extracellular space, V_e in Eq. 5; for V_e we used our value for the sucrose space, 0.274 $\pm$ 0.017 μl/ml, which lies between the values of 0.196 ml/g for sulphate space, obtained by Polimeni (1974) and 0.4 ml/g found for sucrose space by Schafer and Johnson (1964) in edematous myocardium. Translation of myocardial cell diameters of 12 to 17 microns (Berger, 1972) to evenly distributed, infinitely long parallel square beams (as in Fig. 4) using $L = R\sqrt{\pi}$, gave values of L from 10.7 to 15 μm. The limitations on V_e and L limited L_o to a range between 1.5 and 4 μm.

Other considerations provide further limitations:

(*a*) It is most unlikely that the extracellular diffusion of water could be more hindered than that of sucrose, therefore we assume that D_e/D_w° is equal to or a little greater than D_s/D_s°, which was 0.2–0.3, averaging 0.226.

(*b*) The value for D_i/D_w° is not known with any accuracy, but it is likely to be less than the 0.5 found for water in barnacle muscle by Caillé and Hinke (1974) and for a variety of hydrophilic molecules by Kushmerick and Podolsky (1969) inasmuch as their values were for axial diffusion. Radial or transverse diffusion will be slower because most cell constituents, principally the contractile proteins, are aligned at right angles to the diffusional direction of our experiments. Values of 0.1–0.4 probably cover the range. (Values for D_i lower than D_e could occur because of the greater intracellular protein concentrations, and because of the presence of membranes of intracellular organelles.)

(*c*) the permeability P must be moderate, high enough to permit reaching a steady state in <2 h, but not so high that the homogeneous sheet model can be fitted to the data. The shape of the transient portion of $C_R'(t)$ demands that there be some permeability limitation.

(*d*) Because water enters the cells, D_b must be greater than D_b (P = 0) given by Eq. 7 for extracellular diffusion above.

These judgements were utilized in arriving at Fig. 5, in which $D_i = D_e$ and wide limits were used for L and L_o. The reason for plotting calculated D_b, Eq. 6, vs. P was simply to emphasize that P was the parameter about which the least is known and therefore that its estimation should be freed of any preconceived biases. The horizontal lines indicate the mean D_b' $\pm$ 1 SEM, and $\pm$ 1 SD. The values for D_e and for extracellular space V_e govern D_b when P is low, the lower limit being given by Eq. 7. In this set of solutions with $D_i = D_e$, the maximum D_b

at $P = \infty$ is not affected by the geometric parameters governing V_e because diffusion everywhere proceeds at the same rate; this would be the same as the homogeneous sheet model. When $D_i \neq D_e$, the maximum D_b is determined by the D's and L and L_o, as shown by Eq. 8, and is dominated by D_i because intracellular volumes are larger than extracellular.

The figure shows that decreasing the cell size shifts the curves to the right, for the same V_e. Although the surface-to-volume ratio is higher with smaller cells, with smaller cells there are a larger number of permeability barriers along pathway B of Fig. 4.

The range of estimates of P, letting both L and V_e extend over their widest expected range of D_b for 2 SEM, is still quite narrow. The mean P is $\sim 2 \times 10^{-3}$cm/s; using the left and right curves of D_b from Eq. 6 and ± 1 SEM around the mean D_b' defines an envelope (stippled area of Fig. 5) suggesting ± 1 SEM of

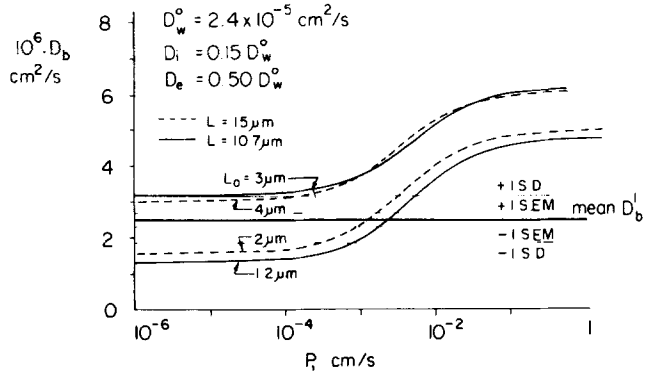

FIGURE 6. Demonstration that $D_e/D_w^\circ < 0.5$: the dashed and continuous curves are solutions of cell-matrix model with $D_i/D_w^\circ = 0.15$, a low estimate, and $D_e/D_w^\circ = 0.5$, an overly high estimate. In the lower range, $P < 10^{-4}$ cm/s, the diffusion could be entirely extracellular and encompass the observed values for D_b'. Because intracellular water must also be included in the diffusion space the figure demonstrates that D_e cannot be as $0.5\ D_w^\circ$.

possible P's at 1 and 4×10^{-3}cm/s. Using the same curves of D_b and ± 1 SD of D_b', the P is estimated to be between 0.5 and 6×10^{-3} cm/s. This envelope gives values of PS, the permeability surface area product ranging from 0.8 to 16 $ml \cdot s^{-1} \cdot g^{-1}$.

These values of P are calculated on the basis that the cell is regular and smooth walled. Bassingthwaighte and Reuter (1972) calculated that the total surface area of the cell was 1.8 times the cylinder surface, due to T tubular invaginations of the sarcolemmal surface. Taking this increased surface area into account raises the estimated cell surface area per gram of tissue, $4L/[(L + L_o)^2 \cdot \rho]$, where $\rho = 1.053$ g/ml (Yipintsoi et al., 1972), from the range of 1,600–2,700 and lowers the estimates of P to about $1.2 \pm 0.8 \times 10^{-3}$cm/s.

Fig. 6 illustrates that impossibly high values of D_e/D_w° must be used to provide a D_b sufficiently high to match D_b' when the permeability is low. With $D_e = 0.5$

D_w°, the observed range of D_b' can be encompassed by the possible range of values of D_b; the slope of the steady-state data can be matched with low P with V_E of 0.3–0.4 ml/ml tissue, but the position (the intercept) cannot. The matching of the slope with this high value for D_e requires omitting transcellular diffusion, which contributes to the observed D_b when P is 10^{-3}cm/s or greater, but this is incompatible with the observed shortness of time to reach the steady state and to equilibrate with the intracellular water, which requires that P be higher than $\sim 10^{-4}$cm/s. The low P condition is the dead-end pore condition, and testing with this model shows that the transient is much too prolonged and the early part of the curve too high for this to be an acceptable solution; the condition is similar to that of the leftmost curve of Fig. 3. The implication of Fig. 6 is therefore that the permeability must be higher than 10^{-4}cm/s and D_e substantially lower than 0.5 D_w°.

Because the sucrose space is ~97.5% of the extracellular water space (Schafer and Johnson, 1964), it is highly unlikely that V_e can be more than a few percent larger than V_{ds}. Similarly, since most of the ECF water is accessible to sucrose, it is highly unlikely that D_e is more than very little greater than $D_s \times D_w^\circ/D_s^\circ$. Acceptance of these arguments puts D_e/D_w° between 20 and 30%. Use of the upper value of 30% for D_e, and assuming D_i to be no higher than D_e would allow only a slightly narrower acceptable range of estimates of P, from ~ 0.8 to 2 × 10^{-3} cm/s, accounting for sarcolemma invaginations as before.

With these various limitations in mind, we have chosen a "best" set of parameter values and computed a "most likely" relationship between D_b' and P, shown in Fig. 7. The input parameters and derived values are given in Table II. The geometric parameters give values for radius of equivalent cylindrical cell = 6.8 μm, smooth cell surface area = 2,300 cm^2/g of tissue, and V_e = 0.265. The value for D_e, 0.22 D_w°, was chosen by analogy to sucrose (Safford and Bassingthwaighte, 1977); D_i = 0.28 D_w° was taken from the $D_{2\text{Corr}}$ of 0.659 ± 0.72 (SD, n = 9) × 10^{-5}cm^2/s from Garrick and Redwood (1977) for water, divided by D_w° of 2.34 × 10^{-5}cm^2/s from McCall and Douglas (1965) translated from 25 to 20°C. From the observed values of D_b', encompassed by the band of stippling on Fig. 7, the curve gave predicted values for the permeability-surface area products, PS, of 7.8 ± 1.3 ml s^{-1}·g^{-1} (SEM, n = 19). Taking an approximate value of S of 4,140 cm^2/g for ventricular myocardium which accounts for T tubular invaginations gives our "best" estimate of the permeability of the sarcolemmal bilayer of 1.9 ± 0.31 × 10^{-3} cm/s (SEM, n = 19).

DISCUSSION

Sources of Error in the Experiments

Unstirred layers on either side of the muscle sheet do not appear to be a problem. Ginzburg and Katchalsky (1963) observed that unstirred fluid layers were only ~ 100 μm thick when stirring was quite ineffective. Dainty and House (1966) considered as "unstirred layers", the sum of the thicknesses of the passive layers of the frog skin plus any unstirred fluid layers. From the time-course of transients in transmembrane potential difference (due to the active transport mechanism) after a change in sodium concentration, they estimated total

thicknesses of stagnant regions to be 30–60 μm, and from potassium transients 100–230 μm. The thickness of the corium (270 μm, Winn et al., 1964) more than accounts for this. If we consider that our stirring rate was about equal to the fastest described in these two studies, and that the position of the bubblers was such that local sweeping of the face of the disc reduced the unstirred layer yet further (Fig. 1, right upper panel), it is reasonable to think that the unstirred fluid layers on each side of the tissue might be only 20–40 μm, certainly <100 μm. However, taking 100 μm as a worst case we can calculate the ratio, r, of the sum of the resistances of the two unstirred layers to the total resistance to diffusion across the sheet, using an equation like Eq. 15 of Safford and

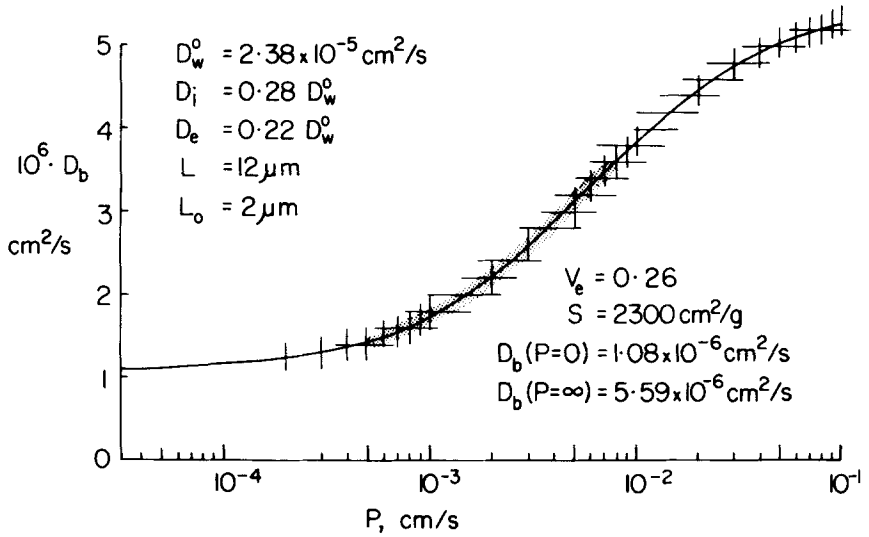

FIGURE 7. Relationship between D_b and P for the cell-matrix model with the most probable set of parameter values. Values are listed in the left upper corner. Estimates of dependent variables are given in the right lower corner. The line is Eq. 6 of the text; the stippling gives the range of observed values of D'_b from Eq. 10. The estimates of permeability-surface area product PS averaged 7.8 ± 1.3 ml·s^{-1}·g^{-1} (SEM, n = 19) and for P, 1.9 ± 0.3 × 10^{-3} cm/s. See Table II.

Bassingthwaighte (1977) and applying it to water, for which the error is larger than for solutes traversing only extracellular pathways:

$$r = \frac{2\Delta x/(D^\circ A_T)}{\bar{l}/(D'_b A_T) + 2\Delta x/(D^\circ A_T)} \leq \frac{2\Delta x}{\bar{l}} \cdot \frac{D'_b}{D^\circ},$$

where Δx is the thickness of the unstirred layer. Substituting values given in Results, $r \leq [2(0.01)/0.15]\cdot[2.5 \times 10^{-6}/2.38 \times 10^{-5}] \leq 0.014$. Thus, neglecting unstirred layers should not cause underestimation of D'_b by even as much as 1.4%.

Edge effects need to be considered in this preparation with small surface area A_T = 0.283 cm^2. One type of potential edge effect is diffusion across the partially

compressed circumferential ring of tissue exposed to the bathing fluids next to the Lucite (E. I. DuPont de Nemours & Co., Wilmington, Del.) O ring (Fig. 1, right upper panel). If flux across the region were at a higher rate than elsewhere, it would increase the levels of $C_R(t)$ and give overestimates of D_b'. The sharpness of the edge of the compressed region of the frozen section (Fig. 1, left panel) suggests that little or none of this region is exposed to the bathing solutions, particularly since the Lucite is coated with a thin layer of silicone grease. Confirming this is the observation that there is a substantial time lag before $C_R'(t)$ deviates detectably from zero, which means there must be a thick layer of tissue between the chambers.

A different type of edge effect is the diffusion of tracer from the disk into the circumferential ring compressed by the Lucite; this must occur to some extent

TABLE II
CELL-MATRIX MODEL

Parameter	Ranges considered (e.g., Figs. 5 and 6)	"Best estimates" (Fig. 7)
D_e/D_w°	0.15–0.50	0.22*
D_i/D_w°	0.15–0.40	0.28‡
L, μm	10.7–15	12§
L_o, μm	1.5–4	2§
V_e, Eq. 5, ml/ml	0.22–0.39	0.265§
S_{smooth}, cm^2/g	‖1,600–2,700	2,300§
$S = 1.8\,S_{smooth}$, $cm^2\,2/g$	‖2,800–4,800	4,140§
$10^6 \cdot D_b$ (observed), Eq. 10, cm^2/s	1.4–3.6	2.5 ± 0.16 (19)¶
$10^6 \cdot D_b$ (P=0), Eq. 7, cm^2/s	0.8–3.1	1.08
$10^6 \cdot D_b$ ($P = \infty$), Eq. 8, cm^2/s	4–7	5.59
PS, Eq. 6, $ml \cdot s^{-1} \cdot g^{-1}$	0.8–16	7.8 + 1.3 (19)¶
$10^3 \cdot P$ (for S_{smooth}), cm/s	‖0.5–6.0	3.4 ± 0.56 (19)¶
$10^3 \cdot P$ (for "true" S), cm/s	‖0.28–3.3	1.9 ± 0.31 (19)¶

* Safford and Bassingthwaighte (1977).
‡ Garrick and Redwood (1977).
§ Equivalent cylindrical cell radius = 6.77 μm; values estimated from Fawcett and McNutt (1969), Page et al. (1971), Polimeni (1974), Bassingthwaighte and Reuter (1972), and Bassingthwaighte et al. (1974).
‖ Fig. 5.
¶ ± SEM (no. of observations).

during the early transient phase. If a significant fraction of the tracer starting across the myocardial disk from the "donor" chamber detoured into this circumferential region, dC_R'/dt would be diminished and the diffusion coefficient underestimated. If tracer entered the compressed region directly from the donor chamber via a fluid-filled slit between the myocardial disk and the compressing lucite, it seems likely that tracer would diffuse across the compressed muscle and into a similar slit on the recipient side, increasing dC_R'/dt (the first type of edge effect) and offsetting to some extent any loss into the compressed region. Our observations in five experiments show that at the end of periods of equilibration of $^1/_2$–4 h, 99.6 ± 0.3% (mean ± SD) of the total tracer was still in the donor chamber, 0.14 ± 0.17% in the recipient chamber,

0.19 ± 0.14% in the disk of myocardium, and 0.02 ± 0.01% in the compressed circumferential region. One would expect the concentration in the compressed region to equilibrate with that halfway through the disk of myocardium, but in fact the values were only 18.4 ± 6.0% as high, presumably mainly because the water content was reduced by the compression, and equilibration was probably incomplete because of the slowness of diffusion into the compressed region. The ratios of amounts of tracer in the compressed region to that in the disk averaged 0.094 ± 0.028. Thus, loss into the compressed region could not lower dC'_R/dt by more than 9.4% even in the transient phase. Therefore, the influence of the steady-state slope on the time lag, T, would be much less than this, probably of the order of 1%.

Homogeneous Sheet and Dead-End Pore Models

Our estimate of D_s at 23°C was 71% of that obtained by Suenson et al. (1974) at 37°C. The Stokes-Einstein theory (Bird et al., 1960) would predict $D^\circ_{s,23°C}/D^\circ_{s,37°C}$ = 85%. Thus, most of the difference between our estimates and those of Suenson et al. (1974) is explained by the reduction of D_s with temperature. Perhaps changes in the geometry of the diffusion channel with temperature could also be affecting the rates. Our estimate was 53% of that of Page and Bernstein (1964), obtained at the same temperature. A possible explanation is suggested by their estimate of sucrose space of 39 ± 14% of tissue water, which is much larger than their estimate of A_{ds} for sucrose diffusion (17 ± 2% of A_T, n = 10). Inasmuch as the product $D_s A_{ds}$ governs the slope dC_R/dt, doubling their estimate of A_{ds} so that it more closely matches the value suggested by the sucrose space, would automatically result in a lowering of their estimate to about the same as ours. (We also note that Page and Bernstein's water curves exhibited "humps" on the upslope which are physically impossible in any stable preparation.)

The dead-end pore model, by providing a "volume" with which diffusing water equilibrated but through which no net flux occurred, provided enough time lag, T, to fit all of the water diffusion curves.

Two physical interpretations of the dead-end pore volume, V_{dep}, have been considered. The first is to consider it as an anatomical volume (e.g., intracellular water) separated from the diffusion channel by a permeability barrier; k_e is then defined as

$$k_e = P S_p / V_{dep},$$

where P is the permeability of the barrier to the diffusing substance and S_p is the surface area of the barrier at the entrance to the "pore". Using the mean values of k_e and V_{dep} from Table I and a muscle water content, V_w, of 0.8 ml H_2O/g muscle we compute the permeability-surface area product, $P S_p$, to be 1.13×10^{-4} cm$^3 \cdot$s^{-1} per gram muscle. Multiplying the estimate by Page et al. (1971) of the surface-to-volume ratio of ventricular cells (3.4×10^3cm^{-1} for the sum of free sarcolemma and T system) and a cellular specific volume of 0.58 cm^3 cells/gram muscle computed from data in Yipintsoi et al. (1972), we find that S_p is of the order of 2,000 cm$^2 \cdot$gm muscle. For a thorough review of dimensions of structures in cardiac muscle see Page and Fozzard (1973).

Therefore, if the dead-end pore is cytoplasmic water we would estimate P to be 6×10^{-8} cm·s^{-1} which is six orders of magnitude smaller than the water permeability for frog skeletal muscle cells reported by Dick (1966). We conclude from this that k_e and V_{dep} cannot be interpreted in terms of a sarcolemmal barrier and total intracellular water.

The second possibility is to consider the dead-end pore as an adsorption site: then the dead-end pore is virtual volume, and k_e would represent the rate of exchange with the sequestered water within the cell. This sequestered intracellular water might be the 20–35% which is suggested to be osmotically inactive or does not act as solvent for ions (Overton, 1902; Gainer, 1968; Blinks, 1965; Hinke, 1970; Sachs and LaTorre, 1974; Grabowski and Bassingthwaighte, 1976). However, Hill (1930), Boyle and Conway (1941), and Dydynska and Wilkie (1963) provided no evidence for water sequestering. The diffusional study of Caillé and Hinke (1974) suggests that 20% of the cytoplasmic water in the giant barnacle, *Balanus nubilus,* is unavailable for intracellular water diffusion. The consensus, with which we agree, is that ~ 20–30% of all water is inactive, but the proposition is certainly not unequivocally proven. This value could explain the dead-end pore volume only if values of P and D_i were as high as proposed using the cell-matrix model. The cell-matrix model accounts for the complexity of the water diffusion "channel" inferred from the simpler modeling. In its present form it provides estimates only from steady-state data. The symmetry of the geometric model of cardiac muscle on which it is based does not account for heterogeneities in cell size and shape. The modeling of molecular diffusion in a direction perpendicular to the long axes of cardiac cells is appropriate to our experimental preparation. The exact geometric arrangement and cell shapes are of little consequence because of the constancy of surface-to-volume ratios for different axisymmetric shapes such as cylinders, square, or hexagonal columns, and because of the short lateral distances, L, for lateral diffusional equilibration. Thus, it appears that the estimation of P is not very sensitive to size and shape, but only to surface area.

We have attempted to choose values of A_{dw}, D_e, and D_i rationally, in accordance with the estimates from models which are sensitive to their variation (our homogeneous sheet and dead-end pore models) and sensible analogy (D_e to D_i); to the extent that we have been successful in this, the cell permeation model then provides estimates of sarcolemmal water permeability. Our estimate of P of 1.9×10^{-3}cm/s is the same as that of Grabowski and Bassingthwaighte (1976) in isolated, Tyrode-perfused beating rabbit hearts using osmotic transient techniques. Obtaining the same estimate from these two totally different techniques gives us some reassurance in feeling that this estimate is reasonable. The value of 1.5×10^{-5}cm/s that Rose et al. (1977) obtained using indicator dilution curves of water, sucrose, and albumin from the coronary outflow in anaesthetized dogs is two orders of magnitude lower. Although it is conceivable that our estimates are abnormally high, our own experiments on blood-perfused beating dog hearts (Yipintsoi et al., 1970) gave the same estimates for sucrose permeability as Rose et al. obtained; the same sets of data showed that capillary water permeabilities were too high to be measured with the multiple indicator dilution technique; i.e., the instantaneous extractions were about 90% and

similar to those for antipyrine and other readily permeating solutes. Highly pertinent to this interpretation is the observation of Yipintsoi and Bassingthwaighte (1970) that antipyrine and water dilution curves are essentially similar at high myocardial blood flows and that a small degree of separation is evident at low flows, the water curves showing slightly (10–20%) higher and earlier peaks; inasmuch as barrier limitations must be more evident at higher flows, the very strong inference is that at low flows the substance of higher diffusibility will be transported via routes less rapidly traversed by one of slower diffusibility. Because water diffuses three times as fast in the myocardium as antipyrine (Winget and Bassingthwaighte, 1978), we conclude that water shows diffusional shunting at low flows, a conclusion based on the anatomic possibilities (Bassingthwaighte et al., 1974) and mathematical analyses (Yipintsoi et al., 1969). Thus, we think the likeliest explanation of the curves of Rose et al. (1977) is that the early part of the water dilution curve that they interpret as a throughput or nonexchanging fraction (e.g., their Fig. 7) is in reality tracer reaching the outflow rapidly by diffusional shunting.

We should emphasize that the modeling of blood-tissue exchange by Rose et al. (1977) is the most advanced available. It is based on the tissue being formed of independent Krogh-type capillary-tissue cylinders and should be suitable for estimating capillary and sarcolemmal permeabilities for potassium or other small hydrophilic solutes where membrane barriers are highly resistive compared to axial diffusion or diffusion between nonidentical regions. However, the modeling may fail to give good estimates when there are diffusional interactions between different capillary-tissue regions and when barrier and intracompartmental diffusional resistivities are of similar magnitude, as they are for water. For example, taking an estimate of the diffusion coefficient of 5×10^{-6}cm^2/s (on the high side) and an estimate of the average intercapillary distance of 20 μm, and considering interstitial diffusion to occur over one-half that distance, one arrives at an equivalent permeability of 5×10^{-3}cm/s. Inasmuch as this value is of the same order as our estimate of the sarcolemmal barrier permeability, it seems reasonable to question whether the multiple indicator dilution curve analysis can give sensitive and accurate estimates of sarcolemmal water permeability. Nevertheless, the technique may be useful, particularly if the permeability in the in vivo situation is much lower than in our preparation.

The water permeability of the dog erythrocyte was estimated by Sha'afi et al. (1971) and by Redwood et al. (1974) to be 5.6 and 5.7×10^{-3}cm/s. If we have overestimated sarcolemma surface area by 50%, we would still have a value of only 2.7×10^{-3}cm/s so it is probably safe to say that myocardial cells are less permeable than erythrocytes. The estimates would be a little closer if we had overestimated D_i, which could be low on account of the need to permeate membranes of mitochondria and sarcoplasmic reticulum.

Garrick and Redwood (1977), in an article published while this one was under review, modified the interpretation of the apparent permeability of the cell ends of the model of Redwood et al. (1974), with the same idea in mind as in our modeling, that is, to account for the extracellular component of the diffusion along pathway B of Fig. 4. We have not tested the accuracy of their approximation against our model solutions, but it is directionally correct. They estimated

the permeabilities of lung cells to water to be 2.9×10^{-3} cm/s, a value which would have been only 2% lower if the extracellular pathway in route B were not accounted for. (However, the underestimation for hexanol, whose permeability was 20×10^{-3} cm/s, was 40%.) Whether their separated, packed cells stored in polyethylene tubes for 2–3 h have physiologically normal permeabilities is not assured, but they demonstrated membrane integrity by the failure of trypan blue to enter the cells. Of relevance to our study is the result that the plasmalemmal permeabilities of a mixture of isolated endothelial and epithelial cells are similar to those of myocardial cells. These are not completely independent, for we have chosen to use their value for D_i (0.28 D_w°, as in Fig. 7) in preference to our previous, less knowledgable estimate used in Fig. 5 (0.25 D_w°). We should keep in mind the possibility that 0.28 D_w° is higher than the effective intracellular D_i, because the repeated freezing and thawing technique that Garrick and Redwood used to prepare material for measuring D_i presumably disintegrates the membranes of the intracellular organelles as well as the plasmalemma. Offsetting this concern are the observations of Caillé and Hinke (1974) in barnacle muscle showing axial diffusion coefficients (which would be expected to be higher than transverse ones) to range from 0.31 to 0.55 D_w°, the lower values being in dehydrated cells.

Stroeve et al. (1976) have developed a model which is conceptually similar: it is devised for carrier-facilitated diffusion in heterogeneous media consisting of spheres uniformly dispersed in a homogeneous phase. Because of the geometric differences their model was not applied to our data. Nevertheless, the mathematical approach that they used is valuable, for it can account for concentration-dependent apparent diffusion coefficients.

The cell-matrix model we presented here is of very simple form but at this stage is the only one available for describing diffusion of substances permeating and diffusing through cells arrayed in oriented fashion within a homogeneous extracellular matrix. Further refinements are readily envisaged: heterogeneity of cell sizes and separations, anisotropy of the diffusion coefficient, and the development of the equations for the transient.

In summary, the values for the bulk diffusion coefficients and the time lag for diffusion are both too high for extracellular diffusion alone, forcing us to conclude that transcellular diffusion makes an important contribution to water diffusion in the myocardium. Furthermore, for this to occur sarcolemmal permeability must be in the neighborhood of 10^{-3} cm/s.

Note Added in Proof Dr. Pieter Stroeve, University of Buffalo, Buffalo, N. Y., in collaboration with us, has developed the equations for two other forms of the heterogeneous cell-matrix model, both using uniform-sized, cylindrical cells, instead of our square cross sections: one form with a square arrangement of cells, as in our model; and the other with a random arrangement. Both versions gave estimates of sarcolemmal P essentially similar to our model.

APPENDIX I

List of Symbols and Abbreviations

A_d	Area of tissue sheet available for diffusion, cm²
A_T	Total area of one side of muscle sheet exposed to solution, cm²

C_D	Counting rate ("concentration") of tracer in donor chamber, counts per $min^{-1} \cdot cm^{-3}$
$C_e(z), C_i(z)$	Counting rate ("concentration") of tracer water in extracellular and intracellular space, counts per $min^{-1} \cdot cm^{-3}$
$C_R(t)$	Counting rate ("concentration") of tracer in recipient chamber, counts per $min^{-1} \cdot cm^{-3}$
$C'_R(t)$	Normalized $C_R(t)$, equal to $C_R(t)/C_D$, dimensionless
D	Diffusion coefficient, $cm^2 \cdot s^{-1}$
D_b, D'_b	Bulk diffusion coefficients for water, defined by Eq. 6 for the cell-matrix model, and experimentally using Eq. 10
D_e, D_i	Extracellular and intracellular diffusion coefficients for water, $cm^2 \cdot s^{-1}$ used in cell-matrix model
D_s, D_w	Sucrose and water diffusion coefficients in tissue, $cm^2 \cdot s^{-1}$
D°_s, D°_w	Sucrose and water diffusion coefficients in free solution, $cm^2 \cdot s^{-1}$
ECF	Extracellular fluid
f	Fractional water content of tissue, ml of H_2O/g of wet muscle
J_w	Steady-state diffusional flux defined by Eq. III.8 and III.9, $mol \cdot s^{-1}$
k_e	Rate constant for exchange between V_d and V_{dep}, s^{-1}
L	Edge length of end of a cardiac cell for model defined in Fig. 4, cm
L_o	Thickness of extracellular space for model defined in Fig. 4, cm
$\bar{l}$	Mean thickness of muscle sheet, cm
l_i	Local thickness of muscle sheet, cm
N, M	Total number of elements in a series, $\sum_{i=1}^{N}$, etc.
P	Sarcolemmal permeability to water, $cm \cdot s^{-1}$
ρ	Myocardial density, 1.053 g/cm^2
R	Constant defined by Eq. III.11, dimensionless
S	Cell surface area, cm^2/g, equal to $4L/[(L + L_o)^2 \cdot \rho]$ for the cell-matrix model
SD, SEM	Standard deviation, standard error of the mean
t	Time, the independent variable, s
T	Time lag for diffusion, s
THO	Tritiated water, ^3HOH
V	Volume of chamber in diffusion cell, cm^3
V_d	Volume of diffusion channel, equal to $A_d \cdot \bar{l}$, cm^3
V_{dep}	Total volume of dead-end pores in tissue slab, cm^3
V_{ds}, V_{dw}	Volume of sucrose and water diffusion channels, cm^3
V_e	Extracellular fluid volume fraction of tissue volume is $1 - L^2/(L + L_o)^2$, ml/ml
V_w	Total tissue water content, cm^3
w_i	Weighting function for calculation of mean tissue thickness, equal to the fraction of the total number of tissue thickness measurements for an experiment that is of magnitude l_i, dimensionless
z	Coordinate direction in which diffusion occurs, see Fig. 4, cm
λ_s, λ_w	Tortuosities $\lambda = (D^\circ/D)^{1/2}$ for sucrose and water, dimensionless

APPENDIX II

Equations for Diffusion through Homogeneous Media

Slab of Uneven Thickness

Following Barrer (1953) and Crank (1956) and considering the diffusion to occur across a set of parallel and independent pathways of length l_i and fractional occurrence w_i

(where $\sum w_i = 1.0$), the following equation was derived by Suenson et al. (1974):

$$C'_R(t) = \frac{DA_d t}{V}\sum_{i=1}^{N}\left(\frac{w_i}{l_i}\right) - \frac{lA_d}{6V} - \frac{2A_d}{\pi^2 V}\sum_{i=1}^{N}\sum_{m=1}^{M}\frac{(-1)^m w_i l_i}{m^2}\exp\left(\frac{-Dm^2\pi^2 t}{l_i^2}\right) \qquad \text{(II.1)}$$

This provides the estimates of the diffusion coefficient and the fractional area available for diffusion from the steady-state slope $(dC'_R/dt)_\infty$, the time lag, T, which is the abscissal intercept shown in Fig. 1, and the thickness distribution, as from Fig. 2:

$$D = \frac{\bar{l}}{6T\sum_{i=1}^{N}\frac{w_i}{l_i}}; \qquad \text{(II.2)}$$

$$A_d = 6VT(dC'_R/dt)/\bar{l}. \qquad \text{(II.3)}$$

A value M of 20 in the third term of Eq. II.1 sufficed. This equation was fitted to all water and sucrose curves; an example is shown in Fig. 1.

Dead-End Pore Model in an Uneven Slab

From Goodknight and Fatt (1961), the modification of Eq. 20—corrected for a typographical error, for the uneven slab composed of independent parallel pathways gives the amount of tracer in the recipient chamber—is:

$$\begin{aligned} VC'_R(t) = {} & DA_d t\sum_{i=1}^{N}\left(\frac{w_i}{l_i}\right) - \left[\frac{V_d + V_{dep}}{6}\right] \\ & + \pi DA_d\sum_{i=1}^{N}\left(\frac{w_i}{l_i^2}\right)\sum_{m=1}^{M}\left[\frac{m(-1)^m\exp(G_i t)}{G_i^2\frac{\partial\beta_i}{\partial G_i}}\right] \end{aligned} \qquad \text{(II.4)}$$

V_{dep} is the total dead-end pore volume of the muscle sheet and V_d (equal to $A_d\bar{l}$) is the volume of the diffusion channel, and G_i and $\partial\beta_i/\partial G_i$ of the transient term (the third) contain the geometric terms plus the rate constant K_e for the exchange between V_{dep} and V_d. (See Safford and Bassingthwaighte, 1977.)

APPENDIX III

Development of the Heterogeneous Cell-Matrix Model

The model is diagrammed in Fig. 4. Diffusion is in the z direction along pathways of types A and B in parallel. Lateral diffusion within ISF or within cells is assumed instantaneous.

Steady-state mass balances on diffusing tracer in an extracellular volume element of thickness dz give rise to two ordinary differential equations for $C_e(z)$. The first,

$$-D_e A_T\frac{d^2C_e}{dz^2} = 0 \qquad (\text{for} \quad -L_o \leqq z \leqq 0), \qquad \text{(III.1)}$$

is valid in the region between the sheets of cells where no exchange between ECF and cells is possible. A_T is the total area of the exposed tissue, cm^2. The second provides for fluxes along the ECF pathway of length L (paths A in Fig. 4) and exchange between cells and ECF:

$$\left(\frac{A_T L_o}{L + L_o}\right)\left(D_e\frac{d^2C_e}{dz^2} + 2PL(C_e(z) - C_i(z))\right) = 0 \qquad (\text{for} \quad 0 \leqq z \leqq L). \qquad \text{(III.2)}$$

Similarly, a mass balance on diffusing tracer within the intracellular volume element yields:

$$\left(\frac{A_T L}{L + L_o}\right)\left(D_i \frac{d^2 C_i}{dz^2} + 2PL(C_i(z) - C_e(z))\right) = 0. \tag{III.3}$$

In the steady state all of the concentrations are constant so that the fluxes can be written directly in continuity equations. Along pathway B, through cells and ECF in series, at the cell membrane:

$$-D_i \frac{dC_i}{dz} = P(C_e(o) - C_i(o)) \quad \text{at} \quad z = 0; \tag{III.4}$$

$$-D_i \frac{dC_i}{dz} = P(C_i(L) - C_e(L)) \quad \text{at} \quad z = L. \tag{III.5}$$

Along both pathways, two additional boundary conditions obtain:

$$C_e = C_e(0) \quad \text{at} \quad z = 0; \tag{III.6}$$

and

$$C_e = C_e(L) \quad \text{at} \quad z = L. \tag{III.7}$$

We begin the solution of this problem by defining the "bulk" tracer water diffusion coefficient for the entire tissue, D_b, in terms of the steady-state diffusional flux, J_w (mol·s^{-1}) across a planar array of tissue elements such as the one indicated by the dashed lines in Fig. 4:

$$J_w = \frac{D_b A_T[C_e(-L_o) - C_e(L)]}{(L + L_o)}. \tag{III.8}$$

Integration of Eq. 5 using the fixed concentrations as boundary conditions yields an alternate expression for J_w:

$$J_w = \frac{D_e A_T[C_e(-L_o) - C_e(L)]}{L_o}. \tag{III.9}$$

Equating Eqs. III.8 and III.9 yields:

$$C_e(-L_o) = \frac{C_e(L) - RC_e(0)}{1 - R}, \tag{III.10}$$

in which

$$R = \frac{D_e}{D_b} \cdot \frac{L + L_o}{L_o}, \tag{III.11}$$

which allows J_w to be redefined in terms of D_b as

$$J_w = \frac{RD_b A_T[C_e(0) - C_e(L)]}{(R - 1)(L + L_o)}. \tag{III.12}$$

The solutions to Eqs. III.2 and III.3 were obtained by the method of trials, obtaining repeated roots from the characteristic equation (the roots being 0, 0, α, and $-\alpha$); the summation of the particular solutions associated with each root provided the solutions for $C_i(z)$ and $C_e(z)$:

$$C_i(z) = k_1 - Wk_2 \cosh(\alpha z) - Wk_3 \sinh(\alpha z) + k_4 z; \tag{III.13}$$

$$C_e(z) = k_1 + k_2 \cosh(\alpha z) + k_3 \sinh(\alpha z) + k_4 z, \tag{III.14}$$

where $W = \left(\frac{L_o}{L}\right)\left(\frac{D_e}{D_i}\right)$, dimensionless;

$$\alpha = \left[2P\left(\frac{1}{LD_i} + \frac{1}{L_oD_e}\right)\right]^{1/2}, \quad \text{cm}^{-1};$$

$$k_1 = C_e(0) - [C_e(0) - C_e(L)]U;$$

$$k_2 = [C_e(0) - C_e(L)]U;$$

$$k_3 = [C_e(0) - C_e(L)]K;$$

$$k_4 = [C_e(0) - C_e(L)]Q;$$

and where U, K, and Q are constants composed of the kinetic and geometric parameters of the model, and which are defined as:

$$K = \frac{1}{J}\left[\frac{1}{E} - \frac{H}{FL}\right], \quad \text{dimensionless};$$

$$U = \frac{1}{F}\left[\frac{1}{L} + GK\right], \quad \text{dimensionless};$$

$$Q = \alpha\left[KW - \frac{U(1+W)}{n}\right], \quad \text{cm}^{-1};$$

where

$n = D_i\alpha/P$, dimensionless; $Y = W[\cosh(\alpha L) + n\sinh(\alpha L)]$, dimensionless;

$$X = W[\sinh(\alpha L) + n\cosh(\alpha L)], \quad \text{dimensionless};$$

$$E = L + D_i/P, \quad \text{cm};$$

$$F = [1 - \cosh(\alpha L)]/L + P(1+W)/D_i, \quad \text{cm}^{-1};$$

$$G = \sinh(\alpha L)/L + W\alpha, \quad \text{cm}^{-1};$$

$$H = (1+Y)/E + P(1+W)/D_i, \quad \text{cm}^{-1};$$

$$I = X/E - W\alpha, \quad \text{cm}^{-1};$$

and

$$J = GH/F + I, \quad \text{cm}^{-1}.$$

Starting from Eq. III.12 we develop an expression defining the bulk diffusion coefficient in terms of the observed flux and the geometric and diffusional parameters. The flux per unit area is defined:

$$j_w = \frac{J_w}{A_T} = \frac{L}{(L+L_o)} \cdot j_i + \frac{L_o}{(L+L_o)} \cdot j_e, \tag{III.15}$$

where the flux per unit area through the extracellular region, pathway A, is j_e and through the cells, pathway B, is j_i:

$$j_i = -D_i\frac{dC_i}{dz}, \tag{III.16}$$

and

$$j_e = -D_e\frac{dC_e}{dz}. \tag{III.17}$$

Differentiating Eqs. III.13 and III.14 and substitution in Eqs. III.16 and III.17 gives:

$$j_i = -D_i[-Wk_2\alpha \sinh(\alpha z) - Wk_3\alpha \cosh(\alpha z) + k_4]; \quad \text{(III.18)}$$

$$j_e = -D_e[k_2\alpha \sinh(\alpha z) + k_3\alpha \cosh(\alpha z) + k_4]. \quad \text{(III.19)}$$

In the steady state the flux across all planes is the same, and at $z = 0$,

$$j_i = -D_i[-Wk_3\alpha + k_4] = -D_i[C_e(0) - C_e(L)][-W\alpha K + Q]; \quad \text{(III.20)}$$

$$j_e = -D_e[k_3\alpha + k_4] = -D_e[C_e(0) - C_e(L)][\alpha K + Q]. \quad \text{(III.21)}$$

Therefore, substituting in Eq. III.15, using Eqs. III.12, III.20, and III.21, gives:

$$\frac{RD_b}{(R-1)(L+L_o)}[C_e(0) - C_e(L)] = \left(\frac{1}{L+L_o}\right)[C_e(0) - C_e(L)][-LD_i(-W\alpha K + Q) - L_oD_e(\alpha K + Q)]. \quad \text{(III.22)}$$

Substituting R from Eq. III.11 in Eq. III.22 yields the bulk diffusion coefficient D_b:

$$D_b = D_e\left\{\left(\frac{L_o}{L+L_o}\right) + \left[L\left(\frac{D_i}{D_e}\right)(W\alpha K - Q) - L_o(\alpha K + Q)\right]^{-1}\right\}^{-1}. \quad \text{(III.23)}$$

The authors are grateful for the assistance of Sylvia Danielson in preparing the manuscript, of Hedi Nurk in preparing the figures, and of Carrol Harris and Dr. Pieter Stroeve in reviewing the manuscript and in providing data on additional cell-matrix models.

This work was supported by grants HL-19139 and HL-19135 from the National Institutes of Health and grant 74-1025 from the American Heart Association and by a Fellowship to Dr. Safford from the Minnesota Heart Association.

Requests for reprints should be directed to Dr. J. B. Bassingthwaighte at the Center for Bioengineering, University of Washington, Seattle, Washington 98195.

Received for publication 23 July 1977.

REFERENCES

BARRER, R. M. 1953. A new approach to gas flow in capillary systems. *J. Phys. Chem.* **57**:35–40.

BASSINGTHWAIGHTE, J. B., and H. REUTER. 1972. Calcium movements and excitation-contraction coupling in cardiac cells. *In* Electrical Phenomena in the Heart. W. C. DeMello, editor. Academic Press, Inc., New York. 353–395.

BASSINGTHWAIGHTE, J. B., T. YIPINTSOI, and R. B. HARVEY. 1974. Microvasculature of the dog left ventricular myocardium. *Microvasc. Res.* **7**:229–249.

BERGER, W. K. 1972. Correlation between the ultrastructure and function of intercellular contacts. *In* Electrical Phenomena in the Heart. W. C. DeMello, editor. Academic Press, Inc., New York. 63–88.

BIRD, R. B., W. E. STEWART, and E. N. LIGHTFOOT. 1960. Transport Phenomena. John Wiley & Sons, Inc., New York. 780 pp.

BLINKS, J. R. 1965. Influence of osmotic strength on cross-section and volume of isolated single muscle fibres. *J. Physiol. (Lond.)*. **177**:42–57.

BOYLE, P. J., and E. J. CONWAY. 1941. Potassium accumulation in muscle and associated changes. *J. Physiol. (Lond.)*. **100**:1–63.

CAILLÉ, J. P., and J. A. M. HINKE. 1974. The volume available to diffusion in the muscle fiber. *Can. J. Physiol. Pharmacol.* **52**:814–828.

CRANK, J. 1956. The Mathematics of Diffusion. Oxford University Press, London. 347 pp.

DAINTY, J., and C. R. HOUSE. 1966. "Unstirred layers" in frog skin. *J. Physiol. (Lond.).* **182**:66–78.

DICK, D. A. T. 1966. Cell Water. Butterworth (Publishers) Inc., Woburn, Mass. 89–98.

DYDYNSKA, M., and D. R. WILKIE. 1963. The osmotic properties of striated muscle fibres in hypertonic solutions. *J. Physiol. (Lond.).* **169**:312–329.

FAWCETT, D. W., and N. S. MCNUTT. 1969. The ultrastructure of the cat myocardium. I. Ventricular papillary muscle. *J. Cell Biol.* **42**:1–45.

GAINER, H. 1968. Osmotically inactive volume of whole frog sartorius muscle: a reappraisal. *Bioscience.* **18**:702–704.

GARRICK, R. A., and W. R. REDWOOD. 1977. Membrane permeability of isolated lung cells to nonelectrolytes. *Am. J. Physiol.* **233**:C104–C110.

GINZBURG, B. Z., and A. KATCHALSKY. 1963. The functional coefficients of the flows of non-electrolytes through artificial membranes. *J. Gen. Physiol.* **47**:403–418.

GOODKNIGHT, R. C., and I. FATT. 1961. The diffusion time-lag in porous media with dead-end pore volume. *J. Phys. Chem.* **65**:1709–1712.

GRABOWSKI, E. F., and J. B. BASSINGTHWAIGHTE. 1976. An osmotic weight transient model for estimation of capillary transport parameters in myocardium. *In* Microcirculation, Vol. 2. Proc. First World Cong. for the Microcirculation. J. Grayson and W. Zingg, editors. Plenum Publishing Corporation, New York. 29–50.

HILL, A. V. 1930. The state of water in muscle and blood and the osmotic behaviour of muscle. *Proc. R. Soc. Lond. B Biol. Sci.* **106**:477–505.

HINKE, J. A. M. 1970. Solvent water for electrolytes in the muscle fiber of the giant barnacle. *J. Gen. Physiol.* **56**:521–541.

IRANI, R. R., and A. W. ADAMSON. 1958. Transport processes in binary liquid systems. I. Diffusion in the sucrose-water system at 25°. *J. Phys. Chem.* **62**:1517–1521.

KING, R. B., and J. B. BASSINGTHWAIGHTE. 1978. Radioactivity. *In* A General Introduction to Instrumentation Techniques in Clinical Medicine. J. Strackee and R. S. Reneman, editors. Martinus Nijhoffs', Gravenhage, Netherlands. In press.

KNOPP, T. J., D. U. ANDERSON, and J. B. BASSINGTHWAIGHTE. 1970. SIMCON-simulation control to optimize man-machine interaction. *Simulation* **14**:81–86.

KUSHMERICK, M. J., and R. J. PODOLSKY. 1969. Ionic mobility in muscle cells. *Science (Wash. D.C.).* **166**:1297–1298.

LAFORCE, R. C. 1967. Device to measure the voltage-current relations in biological membranes. *Rev. Sci. Instrum.* **38**:1225–1228.

MCCALL, D. W., and D. C. DOUGLASS. 1965. The effect of ions on the self-diffusion of water. I. Concentration dependence. *J. Phys. Chem.* **69**:2001–2011.

OVERTON, E. 1902. Beiträge zur allgemeinen Muskel- und Nervenphysiologie. *Pfluegers Archiv Gesamte Physiol. Menschen Tiere.* **92**:115–280.

PAGE, E., and R. S. BERNSTEIN. 1964. Cat heart muscle in vitro. V. Diffusion through a sheet of right ventricle. *J. Gen. Physiol.* **47**:1129–1140.

PAGE, E., and H. A. FOZZARD. 1973. Capacitive, resistive, and syncytial properties of heart muscle—ultrastructural and physiological considerations. *In* The Structure and Function of Muscle, 2nd edition. Vol. II, part 2. G. H. Bourne, editor. Academic Press, Inc., New York. 91–158.

PAGE, E., L. P. MCCALLISTER, and B. POWER. 1971. Stereological measurements of cardiac ultrastructures implicated in excitation-contraction coupling. *Proc. Natl. Acad. Sci. U.S.A.* **68**:1465–1466.

PARADISE, N. F., C. R. SWAYZE, D. H. SHIN, and I. J. FOX. 1971. Perfusion heterogeneity in skeletal muscle using tritiated water. *Am. J. Physiol.* **220**:1107–1115.

POLIMENI, P. I. 1974. Extracellular space and ionic distribution in rat ventricle. *Am. J. Physiol.* **227**:676–683.

REDWOOD, W. R., E. RALL, and W. PERL. 1974. Red cell membrane permeability deduced from bulk diffusion coefficients. *J. Gen. Physiol.* **64**:706–729.

ROSE, C. P., C. A. GORESKY, and G. G. BACH. 1977. The capillary and sarcolemmal barriers in the heart: an exploration of labeled water permeability. *Circ. Res.* **41**:515–533.

SACHS, F., and R. LATORRE. 1974. Cytoplasmic solvent structure of single barnacle muscle cells studied by electron spin resonance. *Biophys. J.* **14**:316–326.

SAFFORD, R. E., and J. B. BASSINGTHWAIGHTE. 1977. Calcium diffusion in transient and steady states in muscle. *Biophys. J.* **20**:113–136.

SCHAFER, D. E., and J. A. JOHNSON. 1964. Permeability of mammalian heart capillaries to sucrose and inulin. *Am. J. Physiol.* **206**:985–991.

SHA'AFI, R. I., C. M. GARY-BOBO, and A. K. SOLOMON. 1971. Permeability of red blood cell membranes to small hydrophilic and lipophilic solutes. *J. Gen. Physiol.* **58**:238–258.

STREETER, D. D., JR., H. M. SPOTNITZ, D. P. PATEL, J. ROSS, JR., and E. H. SONNENBLICK. 1969. Fiber orientation in the canine left ventricle during diastole and systole. *Circ. Res.* **24**:339–347.

STROEVE, P., K. A. SMITH, and C. K. COLTON. 1976. An analysis of carrier facilitated transport in heterogeneous media. *AIChE. J.* **22**:1125–1132.

SUENSON, M., D. R. RICHMOND, and J. B. BASSINGTHWAIGHTE. 1974. Diffusion of sucrose, sodium and water in ventricular myocardium. *Am. J. Physiol.* **227**:1116–1123.

THOMPSON, A. M., H. M. CAVERT, N. LIFSON, and R. L. EVANS. 1959. Regional tissue uptake of D_2O in perfused organs: rat liver, dog heart and gastrocnemius. *Am. J. Physiol.* **197**:897–902.

WINGET, R. R., and J. B. BASSINGTHWAIGHTE. 1978. Diffusion of antipyrine and water through myocardium. *Fed. Proc.* **37**:314. (Abstr.)

WINN, P. M., T. E. SMITH, A. D. CAMPBELL, and E. G. HUF. 1964. Sodium diffusion in epidermis and corium of frog skin and in Ringer-agar gel. *J. Cell. Comp. Physiol.* **64**:371–388.

YIPINTSOI, T., and J. B. BASSINGTHWAIGHTE. 1970. Circulatory transport of iodoantipyrine and water in the isolated dog heart. *Circ. Res.* **27**:461–477.

YIPINTSOI, T., T. J. KNOPP, and J. B. BASSINGTHWAIGHTE. 1969. Countercurrent exchange of labeled water in canine myocardium. *Fed. Proc.* **28**:645. (Abstr.)

YIPINTSOI, T., P. D. SCANLON, and J. B. BASSINGTHWAIGHTE. 1972. Density and water content of dog ventricular myocardium. *Proc. Soc. Exp. Biol. Med.* **141**:1032–1035.

YIPINTSOI, T., R. G. TANCREDI, D. R. RICHMOND, and J. B. BASSINGTHWAIGHTE. 1970. Myocardial extractions of sucrose, glucose and potassium. *In* Capillary Permeability. C. Crone and N. A. Lassen, editors. Munksgaard, Copenhagen. 580–585.